Delamination study of hydroxyapatite coatings for bone orthopedic implants

D. Remache[a], Y. Balcaen [a], I. Demnati [b], D. Grossin [b], J. Alexis [a], G. Bertrand [b], C. Combes [b], C. Rey [b], P. Fort [c], O. Dalverny [a]

a. INPT-ENIT, Toulouse Univ, Tarbes, France, djamel.remache@enit.fr,
b. CIRIMAT, Toulouse Univ, CNRS, Toulouse, France.
c. 2PS, Montbazens, France.

Résumé :

Les revêtements d'hydroxyapatite (HA) des implants orthopédiques sont connus pour leur amélioration de l'ostéointégration et la durabilité de la prothèse en raison de leur compatibilité chimique avec l'os. L'intégrité et la continuité des implants revêtus de HA sont fortement influencées par l'adhérence du revêtement sur le substrat. L'objectif de ce travail est d'étudier les mécanismes d'endommagement des revêtements HA, déposés sur l'alliage de titane TA6V par projection plasma fonctionnant à basse énergie (LEPS). Des essais de traction ont été effectués à cet égard. Les éprouvettes en traction ont été observées lors des tests à l'aide de deux caméras synchronisées, spécialement conçues pour la corrélation d'images numériques. La première caméra était focalisée sur la tranche de l'échantillon, tandis que la seconde était focalisée sur sa face. Ceci nous a permis d'avoir une observation précise des mécanismes d'endommagement du revêtement. Les observations ont montré qu'une importante décohésion du revêtement se produisait avant toute fissuration visible. Un modèle d'éléments finis a été développé pour simuler le délaminage du revêtement survenant au cours de l'essai de traction. La simulation nous a permis de mieux comprendre les mécanismes du délaminage et d'évaluer les paramètres interfaciaux critiques.

Abstract :

Hydroxyapatite (HA) coatings for orthopedic implants are known to enhance the osteointegration and durability of prosthesis due to their chemical compatibility with bone. The integrity and continuity of the HA-coated implants is strongly influenced by the adhesion of the coating to the substrate. The objective of the current work was to investigate the damage mechanisms of HA coatings, deposited onto Titanium alloy TA6V using a plasma spray operating at low energy (LEPS). Tensile tests were performed for this purpose. The tensile specimens were observed during the tests using two synchronized cameras, specifically designed for Digital Image Correlation. The first camera was focused on the edge of the sample, while the second was focused on the face of the sample. This allowed us to perform an accurate observation of the damage mechanisms of the coating. The observations showed that a large decohesion of the coating occurred before any visible cracking. A two-dimensional plane-strain finite element model

was developed to simulate the coating delamination occurring during tensile test. The simulation helped us to better understand the delamination mechanisms and to evaluate the critical interfacial parameters.

Mots clefs : Hydroxyapatite coatings, damage mechanisms, cohesive zone finite element model

1 Introduction

The proper design of a orthopedic implant material is aimed to provide the requisite durability, functionality, and biological response in long term use [1, 17, 18, 20]. Many factors may influence the outcome of such an implant. Among these factors, the bone/implant interface, which appears as a critical zone determining both the initial and long term success of this surgery [1, 17, 18, 20]. Because bone mineral is a natural calcium phosphate ceramic, calcium phosphates, such as hydroxyapatite (HA), ($Ca_{10}(PO_4)_6(OH)_2$), have been widely used to provide bioactive coatings on the metal implant surfaces [24]. Hydroxyapatite (HA) coatings deposited on Titanium and its alloys are considered as the state of the art orthopedic implant materials because of their highly biocompatibility and osseointegration [4, 17, 22]. However, the weak adhesion of the coating to the substrate remains a critical point of this implant material [4, 11, 17, 22].

There are many deposition techniques of coatings on metals [17, 20, 22], such as sputtering, rf-suspension plasma spray, micro-plasma spray, sol gel, pulsed-laser, electrodeposition [1], hydrothermal electrochemical method, etc.... Among these techniques, plasma-sprayed process is the most widely commercially used deposition technique of HA coating on metals because it is a rapid and an inexpensive technique [4, 7, 20]. However, the thermal deposition processes lead to the phase transformation and decomposition of the initial HA powder and the homogeneity and the thickness of the coating are hardely controlled [17, 20, 22], which leads to poor adhesion of the coating on the titanium and therefore to clinical coating failure by chipping and delamination [1, 11, 20].

In the current study, a low-energy plasma spray systems (LEPS), designed by Demnati et al. 2011 [9], was used as a deposition technique to deposit HA coatings on TA6V. The adhesion of the HA coating to the substrate was then investigated. There are many adhesion tests to evaluate coating adhesion on implants, such as pull-off strandard test ASTM F1147 or ISO 13779-4 , blister test, interfacial hardness test, scratch test, bending test, [16, 21, 22]. However, all these techniques are limited to accurately measure the adhesion strength of coating on metals [22]. In this study, due to the process configuration and coating properties, conventional tensile microtests were performed on samples and the coating deformation were analyzed thanks to digital image correlation. Experimental and numerical tools were used to investigate the adhesion properties.

2 Experimental

2.1 Sample preparation

The substrate used for the coating was a Titanium alloy TA6V plate. Six samples were cut, cleaned, degreased and blasted. The shape and dimensions of the samples are shown in Fig. 1. HA powders were plasma sprayed onto substrate samples using a plasma spray operating at low energy (LEPS) [12]. The

deposition was performed in the air with the LEPS equipment (2PS, France) using argon as the only plasma gas. All samples were made under the same thermal spraying conditions [12]. The photography of the coated sample is shown in Fig. 1.

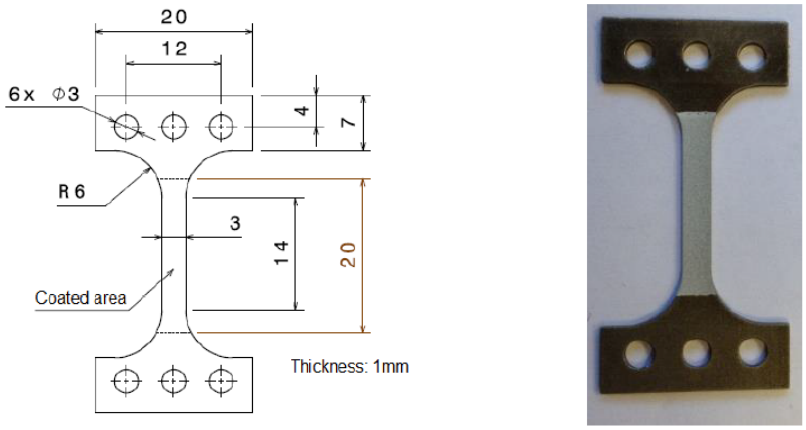

FIGURE 1 – Drawing and dimensions of the tested samples (on the left). Photography of the coated sample (on the right).

2.2 Tensile testing

Tensile tests were performed with a DEBEN MICROTEST (Loadcell, 5 kN) testing machine, provided with gripping systems, ensuring sample alignment. Samples were mounted horizontally and loaded with an extension rate of 1 mm/mn. During testing, the samples were observed using two synchronized cameras, specifically designed for Digital Image Correlation (DIC). The configuration of the cameras with respect to the tested samples is illustrated in Fig. 2. The first camera (2) was focused on the edge of the sample (1), while the second camera (3) records images on its top face. Image acquisition was performed with the ARAMIS ® system, a non-contact and material-independent measuring based on the DIC. This system provided by GOM Company, performs high-precision measurements, such as displacements and surface strain, with a 3D image resolution in the submicrometer. In this study, an accurate observation of the debonding and cracking of the coating was performed and the engineering strain was measured using differential marks displacement thanks to the software included in the ARAMIS system. The measurements were performed on the edge of the sample as a function of the image number. Otherwise, an analysis of the top face images of the sample was performed in order to measure the debonding of the coating as a function of strain. The debonding phenomenon was related to a progressive change in the color contrast on the top surface of the coating. This image analysis was performed with the software ImageJ.

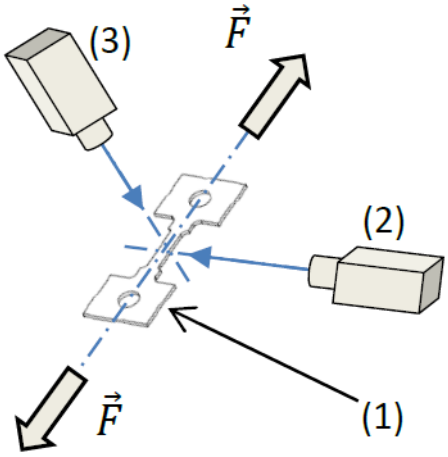

FIGURE 2 – Configuration of the cameras during testing.

2.3 Experimental results

2.3.1 Tensile testing

Thanks to gripping systems, misalignment, which is a common cause of premature failure [16], was avoided and the tensile tests were all valid. The tensile testing results revealed insensitivity of the stress–strain curves to the coating strain. This is obviously due to the large difference of thicknesses and mechanical properties between the coating and the substrate. Thanks to the DIC, performed with the ARAMIS system, the engineering strain of coating was measured and the initial micro-crack for each tested sample was identified. A strain range of 1.46% to 2.3% was measured for the identified initial micro-cracks. On the other hand, image analysis of samples showed that from a certain image (in this case the image 53 in Fig. 3), a color contrast evolution was observed on the surface of the coating. As the sample deformation increased, the coating became more and more bright until its total decohesion (Fig. 3). It was also observed that the cracks start to occur in the brightest area of the coating (Fig. 3) and a coating delamination was observed in these areas (Fig. 4). The change in the color contrast on the top surface of the coating was analyzed using image analysis performed with the software ImageJ. Therefore, we were able to plot the evolution of the delaminated coating as a function as the average strain applied to the Titanium substrate. Fig. 5 shows the coating debonding rate of the tested samples versus the average engineering strain performed.

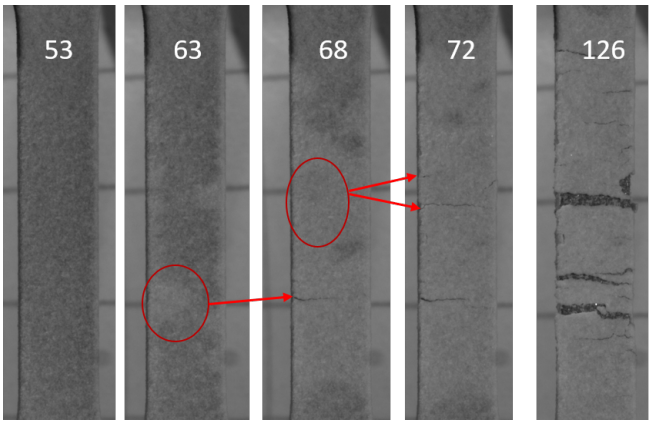

FIGURE 3 – Illustration of the change in the color contrast on the surface of the coating as a function as image number (indicated on each image). The brightest area, framed in red, predicts the area in which the crack will be produced.

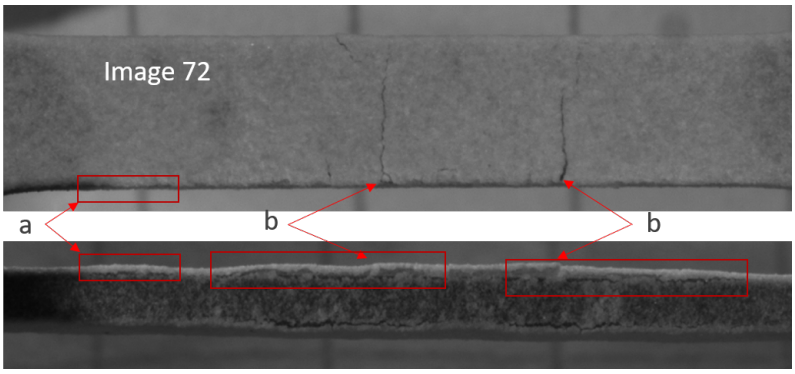

FIGURE 4 – Illustration of the coating delamination far from cracks (a) and close to cracks (b).

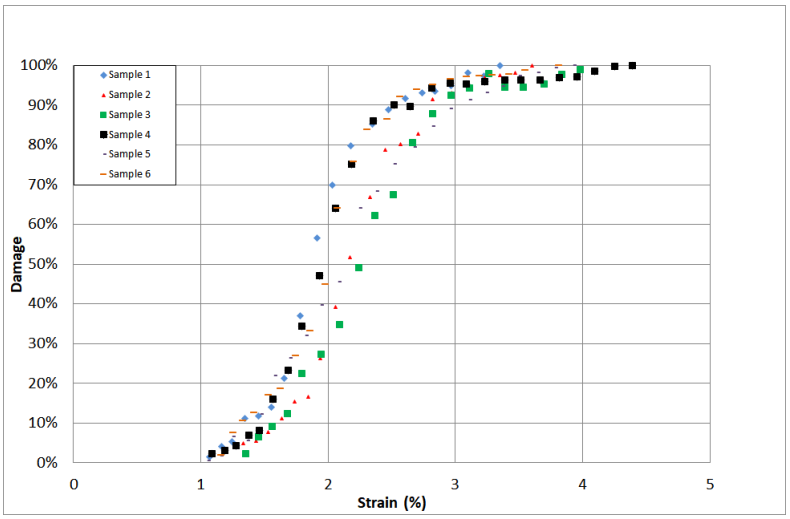

FIGURE 5 – The coating debonding rate of the tested samples, denoted as damage, versus the measured engineering strain performed with DIC.

3 Finite Element analysis

3.1 Finite element model

Based on experimental observations (Fig. 4), we assumed that the coating delamination expanded along the interface on both sides of each crack. The coating delamination in the left side of the initial crack was simulated in order to evaluate this damage. To simplify the calculation, initial crack was assumed to be located at the coating edge. The finite element (FE) analysis was used for simulation. A two-dimensional model was developed in Abaqus ®2018 finite element code. The model consists of two layers : the HA coating and the TAV6 substrate. The interface between the two model layers was considered as the cohesive zone. As illustrated in Fig. 1, the length gauge of the sample is 20 mm and the length of the coated area size is 14 mm. Assuming that the mechanical problem is symmetric with respect to the transversal sample direction, only half of the model was modeled. The thickness of the HA layers was 0.06 mm and the substrate's thickness was 1 mm. The cohesive layer thickness was assumed 1 μm. The finite element mesh and boundary conditions of the model are illustrated in Fig. 6. The 4-node bilinear, type CPE4R, reduced integration, plane strain elements were used for meshing the two model layers, and the 4-node, two-dimensional cohesive element, type COH2D4, was used as element type for meshing the cohesive zone. Finer elements were used in the vicinity of the interface surface. The nonlinear analysis procedure was used in the calculation steps. Tie constraints were imposed between the cohesive zone and the two layers interfaces. An uniform axial displacement was applied on the right side and zero displacement was imposed to the opposite side, at which the symmetry boundary was applied.

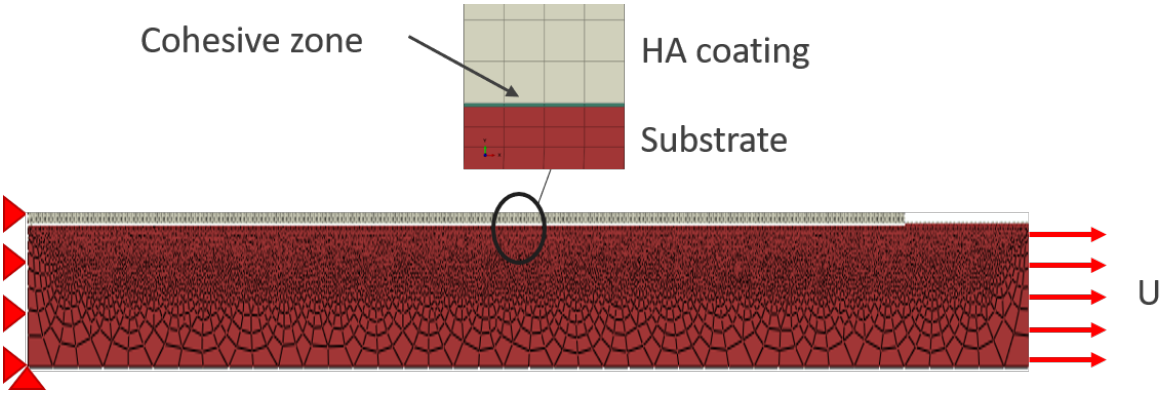

FIGURE 6 – The finite element mesh and boundary conditions of the model.

As mechanical properties, the coating was assumed isotropic material and the substrate isotropic homogenous elastic–plastic material with nonlinear strain hardening. The mechanical properties of the coating (Table 1) were determined using nanoindentation testing, which is not presented in this work. The constitutive model proposed by Johnson–Cook (JC) [19] was chosen for the substrate. The flow stress of the JC model is given by the following relationship :

$$\sigma = \begin{cases} \left[A + B\varepsilon_p^n\right]\left[1 + C\ln\left(\frac{\dot{\varepsilon}}{\dot{\varepsilon}_0}\right)\right]\left[1 - T^{*m}\right] \\ T^* = \frac{T - T_0}{T_m - T_0} \end{cases} \tag{1}$$

where ε_p is the equivalent plastic strain, $\dot{\varepsilon}$ and $\dot{\varepsilon_0}$ are the plastic strain rate and the reference plastic

TABLE 1 – The mechanical properties of the substrate and coating.

Material	E (GPa)	ν	A (GPa)	B (GPa)	n
HA	60	0.3	-	-	-
TA6V	104.160	0.3	0. 693	0.566	0.44

strain rate, respectively. T^* is the normalized temperature ; T_0 is a reference temperature, and T_m is a reference melt temperature. A , B, n, C, and m are the material constants. The expression in the first set of brackets gives the stress as a function of strain for $\dot{\varepsilon} = \dot{\varepsilon_0}$ and $T^* = 0$. A is the yield stress ; B is the strain hardening modulus and n is the strain hardening exponent. The expressions in the second and third sets of brackets represent the effects of elevated strain rates and temperature, respectively. Since the experimental tensile test was a quasi-static test without significant thermal changes, the second and third factor in the constitutive relationship were neglected. The constants (Table 1) in the first set of brackets were determined using the inverse method.

3.2 Cohesive zone model (CZM) approach

As stated above, a cohesive zone model was chosen to predict the initiation and progression of delamination at the interface. The constitutive response of the cohesive elements was defined in terms of a the bilinear traction-separation law graphically depicted in Fig. 7 and described [8, 27] according to the following relationships :

$$\sigma_i = \begin{cases} K\,\delta_i, & \delta_i \leq \delta_i^0 \\ (1 - D_i)\,K\delta_i, & \delta_i^0 < \delta_i < \delta_i^{\mathrm{f}},\ (i = n,\, s)\,, \\ 0, & \delta_i \geq \delta_i^{\mathrm{f}} \end{cases} \tag{2}$$

$$D_i = \begin{cases} 0 & \delta_i \leq \delta_i^0 \\ \frac{\delta_i^{\mathrm{f}}\left(\delta_i - \delta_i^0\right)}{\delta_i\left(\delta_i^{\mathrm{f}} - \delta_i^0\right)}, & \delta_i^0 < \delta_i < \delta_i^{\mathrm{f}},\ (i = n,\, s)\,, \\ 1 & \delta_i \geq \delta_i^{\mathrm{f}} \end{cases} \tag{3}$$

$$G_{ic} = \frac{1}{2}\sigma_i^0 \delta_i^{\mathrm{f}},\ (i = n,\, s) \tag{4}$$

were σ_i and δ_i are the stress and nominal strain components, σ_i^0 is the stress at damage initiation, δ_i^0 and δ_i^{f} are the nominal strain components at damage initiation and failure, respectively. D is the scalar damage variable, K is the interface stiffness. G_{ic} are the critical fracture energies. Subscripts n and s represent normal and shear directions.

The damage evolution is defined in terms of energy. The quadratic nominal stress criterion was introduced to determine the damage initiation [3, 8]. This criterion can be represented as :

$$\left(\frac{\langle \sigma_n \rangle}{\sigma_n^0}\right)^2 + \left(\frac{\sigma_s}{\sigma_s^0}\right)^2 = 1 \tag{5}$$

where :

$$\langle \sigma_n \rangle = \begin{cases} \sigma_n, & \sigma_n \geq 0 \\ 0, & \sigma_n \leq 0 \end{cases} \tag{6}$$

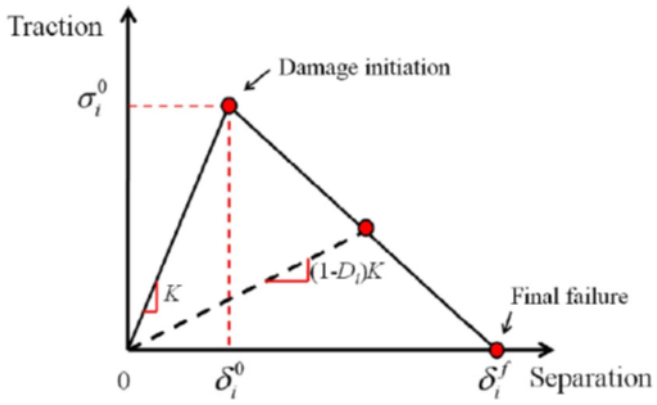

FIGURE 7 – The traction–separation law response of the cohesive element [27].

According to Benaqqa et al. [2], the HA fracture toughness values range between 0.95 MPa $\sqrt{\text{m}}$ to 1.2 MPa $\sqrt{\text{m}}$. In this study, a value of 1 MPa $\sqrt{\text{m}}$ [24] was chosen as HA fracture toughness. The corresponding critical fracture energy is therefore 16.7 J/m^2, which was taken for the interface. Also, According to Benaqqa et al. [2] the fracture strength of the HA range between 50 MPa to 196 MPa. The nominal stress values in normal and shear directions were varied thus from 50 MPa to 200 MPa in the the simulation procedure until the target curve is reached. For the interface stiffness, K, the value of 10^4 N/mm^3 was taken from Zhao et al. [26].

3.3 Numerical results

The simulation of the sample response to tensile loading is shown in Fig. 8, which clearly shows the coating delamination. The damage evolution in cohesive elements is expressed in the term of the scalar stiffness degradation, SDEG, which evolves from 0 to 1 once the initiation criterion is reached. When SDEG reaches the value 1, the cohesive element is deleted. The average overall response of the damaged cohesive zone elements was calculated for different values of nominal stress as mentioned above, then, for each calculation, the obtained curve damage-strain was compared to the experimental curves (Fig. 5) until the fitting of curves is reached. Two tangent curves to the experimental curves are presented in Fig. 9. The curve, denoted Sim 1, corresponds to 160 MPa 150 MPa of nominal stress values in normal and shear directions, respectively, the curve, denoted Sim 2, corresponds to 180 MPa and 170 MPa of nominal stress values in normal and shear directions, respectively.

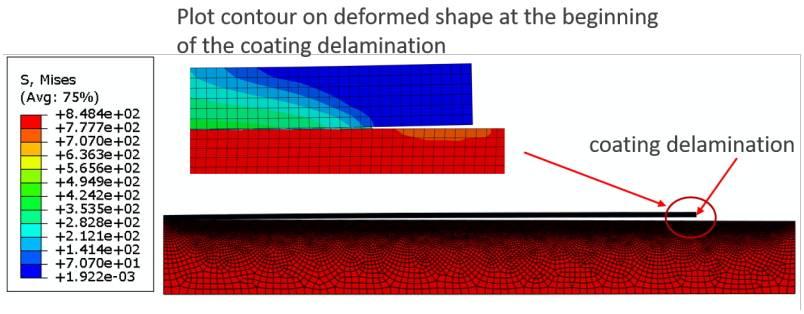

FIGURE 8 – Deformed geometry after the coating debond.

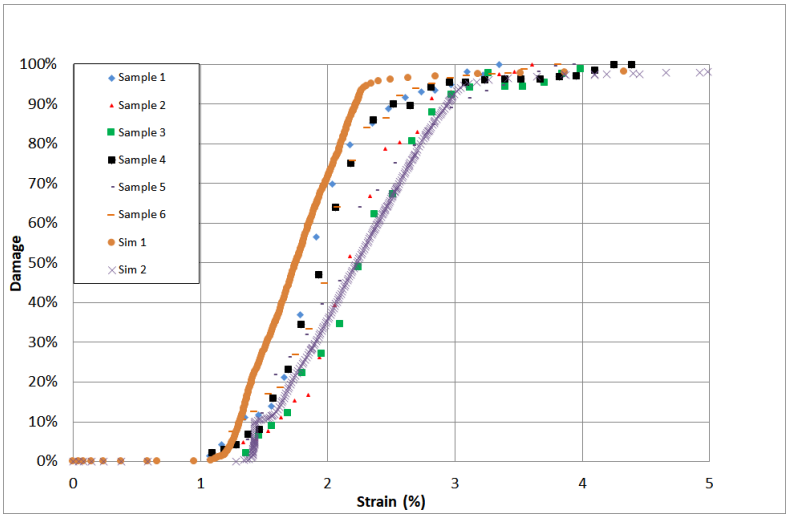

FIGURE 9 – Numerical and experimental damage-strain curves.

4 Discussion

The main factors in determining the adhesion quality of HA coatings are the coating thickness, the degree of crystallinity and porosity. Ideal HA coatings should be uniform in thickness, with a high degree of crystallinity and low porosity at the substrate-coating interface [11, 12, 17, 22]. Indeed, the HA coatings with poor crystallinity can be easily dissolved, causing a decrease in adherence to the substrate [17]. Very thin HA coatings may resorb faster than thicker coatings, whereas, fatigue failure usually occurs in the thicker coatings [23], which may have a high level of porosity [12]. An optimum thickness of 50 -75 µm would thus avoid resorption and fatigue failure [23]. It has also been shown that the failure strength increases as coating thickness decreases [16, 22]. These factors depend mainly on the coating deposition process [22, 23].

The current study is the continuation of the work performed by Demnati et al. [12, 10]. In this previous study, a novel LEPS device, designed by Demnati et al. 2011 [9], was used as HA coating deposition process on TA6V. This technique has shown its ability to form a thin film of HA with high crystallinity and good homogeneity. The microstructure and composition of the HA coatings of the tested samples were explained and discussed in [12]. An average coating thickness of about 60 µm was measured on cross sections of the tested samples, which is an optimal value according to the above discussion.

There are two mode of delamination processes, cohesive failure and adhesive failure. A cohesive fai-

lure occurs in the coating bulk while an adhesive failure occurs at the interface between the coating and the substrate [13]. The damage mechanism of the HA coating under tensile testing was evaluated with image analysis. During deformation, a change in the color contrast on the surface of the coating was observed (Fig. 3). This change was related to the coating debonding from the substrate. So, an interfacial delamination occurs before any crack initiation, then extends from the initial cracks with the applied strain. The micro-cracks generally occur and grow in the coating perpendicular to the loading direction (Fig. 4). The debonding rate versus the measured engineering strain gave an exponential curve (Fig. 5), which illustrates the fast progression of the delamination after damage initiation. During tensile testing, strains are transmitted to the coating. It was shown that the initial micro-cracks were identified at a minimum 1.46% of strain. This strain phase corresponds to the plastic deformation phase of the substrate, which is greater than 1%. For such deformation, the coating adhesion to the substrate can't overcome the tensile strength of the ductile substrate. This shows that the coating has a great adhesion. Therefore, the tensile testing applied to the samples induce the two damage mechanisms of the HA coatings, the adhesive failure at the interface between the coating and the substrate and the cohesive failure in the coating bulk. The two damage mechanisms of the HA coatings are certainly due to the coating defects such as cracks and pores as it has been usually observed [1, 23].

The adhesion strength is the maximum tensile strength corresponding to the damage initiation [17]. The adhesion strength values reported in the literature for HA coated Titanium and its alloys varied between 5 and 80 MPa [17]. The highest value has been reached using the sputtering deposition technique [22]. The tensile adhesion strength of HA plasma-sprayed has been estimated in a range of about 25 MPa [17, 22] but, according to Yang et al. [25], the minimal values of the tensile strength and shear strength required for HA coats are 50.8 MPa and 22 MPa, respectively. Nevertheless, until now, there is a limitation of research discussing the optimal adhesion strength required for HA coatings.

In the current study, the tensile adhesion strength was evaluated numerically, based on experimental results. The interface between the coating and the substrate was modeled with the cohesive zone model and the cohesive elements behavior was compared to the coating debonding. As shown in (Fig. 9), a good prediction of the coating delamination was obtained. The identified values of the nominal stresses (in the range of 150 to 180 MPa) seem to be too high values compared to the values discussed above. However, these values were extracted using a non-contact method (i.e. image analysis) that has never been used before to characterize the HA coating delamination, to the best of our knowledge, in addition a novel process was used for coating. Finally, the LEPS process has shown its ability to form a film of HA with great adhesion.

5 Conclusions

The objective of the current study was to investigate the damage mechanisms of HA coatings deposited on TA6V substrate using LEPS process and to evaluate its adhesion strength. The microtensile tests performed on HA coated Titanium showed that the coatings failure occurs in the plastic deformation phase of the Titanium substrate, which shows that the coating has a good adhesion strength. An interfacial delamination was observed before critical cracks are initiated, then, from the initial cracks, the delamination extends along the interface with the applied strain. The micro-cracks generally occur and grow in the coating perpendicular to the loading direction. A cohesive zone finite element model has been developed to predict the mechanical behavior of the interface between the HA coating and the

Titanium substrate. The cohesive elements behavior was compared to the experimental coating debonding. The values of the nominal stresses in the range of 150 to 180 MPa were predicted, showing the high adhesion of the coating to the substrate.

Remerciements

Ce travail de recherche est soutenu par le projet de recherche scientifique ArchiCaP « Architectured substituted calcium phosphate coatings for bioactive bone implants », financé par l'Agence Nationale de Recherche (ANR).

Références

[1] R.I.M. Asri and W.S.W. Harun and M.A. Hassan and S.A.C. Ghani and Z. Buyong, A review of hydroxyapatite-based coating techniques : Sol-gel and electrochemical depositions on biocompatible metals, Journal of the Mechanical Behavior of Biomedical Materials, 2016.

[2] C.Benaqqa, J. Chevalier, M. Saadaoui, G. Fantozzi, Slow crack growth behaviour of hydroxyapatite ceramics, Biomaterials, 2005.

[3] P. P. Camanho, C. G. Davila, M. F. de Moura, Numerical Simulation of Mixed-Mode Progressive Delamination in Composite Materials , Journal of Composite Materials, 2003.

[4] M. Chambard, O. Marsan, C. Charvillat, D. Grossin, P. Fort, C. Rey, F. Gitzhofer, G. Bertrand, Effect of the deposition route on the microstructure of plasma-sprayed hydroxyapatite coatings, Surface and Coatings Technology, 2019.

[5] M. Chambard, O. Marsan, C. Charvillat, D. Grossin, P. Fort, C. Rey, F. Gitzhofer, G. Bertrand, Effect of the deposition route on the microstructure of plasma-sprayed hydroxyapatite coatings, Surface and Coatings Technology, 2019.

[6] M. Chambard, O. Marsan, C. Charvillat, D. Grossin, P. Fort, C. Rey, F. Gitzhofer, G. Bertrand, Effect of the deposition route on the microstructure of plasma-sprayed hydroxyapatite coatings, Surface and Coatings Technology, 2019.

[7] Q.Y Chen, Y.L Zou, X. Chen, X.B. Bai, G.C. Ji, H.L. Yao, H.T. Wang, F. Wang, Morphological, structural and mechanical characterization of cold sprayed hydroxyapatite coating, Surface and Coatings Technology, 2019.

[8] C Davila, P Camanho, Analysis of the effects of residual strains and defects on skin/stiffener debonding using decohesion elements, 44th AIAA/ASME/ASCE/AHS/ASC Structures, Structural Dynamics, and Materials Conference, 2003.

[9] I. Demnati, Développement et caractérisation de revêtements bioactifs d'apatite obtenus par projection plasma à basse énergie : application aux implants biomédicaux, Univ. Toulouse, 2011.

[10] I. Demnati, D. Grossin, C. Combes, M. Parco, I. Braceras, C. Rey, A comparative physicochemical study of chlorapatite and hydroxyapatite : from powders to plasma sprayed thin coatings, Biomedical Materials, 2012.

[11] I. Demnati, D. Grossin, C. Combes, C. Rey, Plasma-sprayed apatite coatings : review of physical-chemical characteristics and their biological consequences, Journal of Medical and Biological Engineering, 2014.

[12] I. Demnati, M. Parco, D. Grossin, I. Fagoaga, C. Drouet, G. Barykin, C. Combes, I. Braceras, S. Goncalves, C. Rey, Hydroxyapatite coating on titanium by a low energy plasma spraying minigun, Surface and Coatings Technology, 2012.

[13] J.M. Fernandez-Pradas, L. Cleries, e. Martinez, G. Sardin, J. Esteve, J.L. Morenza, Influence of thickness on the properties of hydroxyapatite coatings deposited by KrF laser ablation, Biomaterials, 2001.

[14] M.J Filiaggi, N.A Coombs, R.M Pilliar, Characterization of the interface in the plasma-sprayed HA coating/Ti-6Al-4V implant system, Journal of Biomedical Materials Research, 1991.

[15] R. Gadow and A. Killinger and N. Stiegler, Hydroxyapatite coatings for biomedical applications deposited by different thermal spray techniques, Surface and Coatings Technology, 2010.

[16] D. Hardwick, The mechanical properties of thin lms : A review, Thin Solid Films, 1987.

[17] W.S.W.Harun, R.I.M.Asri, J.Alias, F.H. Zulkifli, K. Kadirgama, S.A.C.Ghani, J.H.M. Shariffuddine, A comprehensive review of hydroxyapatite-based coatings adhesion on metallic biomaterials. Ceramics International, 2018.

[18] J.A. Helsen, H.J Breme, Metals as biomaterials, Wiley, 1998.

[19] G. R Johnson, W. H Cook, A constitutive model and data for metals subjected to large strains, high strain rates and high temperatures, In : Proceedings of the 7th International Symposium on Ballistics, 1983.

[20] C. Massaro, M. Baker, F. Cosentino, P. Ramires, S. Klose, E ; Milella, Surface and biological evaluation of hydroxyapatite-based coatings on titanium deposited by dierent techniques. Journal of Biomedical Materials Research, 2001.

[21] T. Mohammadi, B.Wan, K. Harries, Intermediate crack debonding model of frp-strengthened concrete beams using xfem. In : SIMULIA Community Conf., Dassault Systemes, Paris, 2013.

[22] E. Mohseni, E. Zalnezhad, A. Bushroa, Comparative investigation on the adhesion of hydroxyapatite coating on ti-6al-4v implant : A review paper. International Journal of Adhesion and Adhesives, 2014.

[23] Y. Su, K. Li, L. Zhang, C. Wang, Y. Zhang, Effect of the hydroxyapatite particle size on the properties of sprayed coating, Surface and Coatings Technology, 2018.

[24] HJA. Van Dijk, N. Hattu, K. Prijs, Preparation, microstructure and mechanical properties of dense polycrystalline hydroxy apatite, Journal of Materials Science, 1981.

[25] Y. Yang, KH. Kim, JL. Ong, A review on calcium phosphate coatings produced using a sputtering process-an alternative to plasma praying, Biomaterials, 2005.

[26] L. Zhao, Y. Gong, J. Zhang, Y. Chen, B. Fei, Simulation of delamination growth in multidirectional laminates under mode i and mixed mode i/ii loadings, Composite structures, 2014.

[27] W. Zhu, L. Yang, JW. Guo, YC. Zhou, C. Lu , Determination of interfacial adhesion energies of thermal barrier coatings by compression test combined with a cohesive zone finite element model, International Journal of Plasticity, 2015.